Research on Engineering Structures & Materials
www.jresm.org
Research Group

Research Article

Optimization of whirl milling parameters based on multi-objective optimization and vibration control

Xiaona Li [*,1,a], Xiang Du [2,b]

[1]*Engineering Training Center, Shandong Huayu University of Technology, Dezhou, 253000, China*
[2]*Teaching Quality Monitoring and Evaluating Center, Shangdong Huayu University of Technology, Dezhou, 253000, China*

Article Info

Article History:

Received 30 Jul 2026

Accepted 28 Sep 2026

Keywords:

Whirl milling;
Parameter optimization;
Multi-objective optimization;
Vibration control;
IMOGWO

Abstract

In the optimization of whirl milling parameters, traditional methods often suffer from chatter instability due to ignoring dynamic physical boundaries, which makes it difficult to coordinate processing efficiency, quality and stability. To this end, the study proposes an optimization solution that integrates physical models and improved intelligent algorithms. At the model level, a stability hard constraint based on the regenerative flutter mechanism is constructed, and the physical safety boundary is internalized as the search premise of the algorithm. At the algorithm level, an improved multi-objective gray wolf optimization algorithm is designed, which improves search diversity by integrating chaotic mapping, and uses an adaptive penalty mechanism to deal with strong nonlinear constraints. The results show that the typical solution without constraints has an energy peak of 0.95 at the chatter frequency of 1500Hz, while the energy distribution of the constrained optimization solution remains flat. In the algorithm comparison, the inverted generational distance distribution range of the improved optimization algorithm is 0.03-0.07, and the average vibration amplitude of the finally obtained Pareto solution set is suppressed to about 0.18mm. Meanwhile, the solution set quality of the improved optimization algorithm after about 150 iterations has surpassed the final results of other algorithms after 500 iterations. In summary, the proposed optimization scheme integrating physical constraints and intelligent algorithms provides a new idea for solving the stability conflict of highly dynamic whirl milling, and achieves efficient and stable parameter optimization results under the given computational and experimental conditions for this category of parts.

© 2026 MIM Research Group. All rights reserved.

1. Introduction

With its advantages of high efficiency and high precision, whirl milling technology has become the core process for processing key components such as TC4 titanium alloy ball screws in the fields of aerospace and precision transmission [1-2]. However, the optimal selection process of this process parameter faces the challenge of multiple physical constraints and complex performance trade-offs. On the one hand, there are obvious inherent conflicts between core performance indicators such as processing efficiency and surface quality, which constitutes a typical multi-objective optimization problem [3]. On the other hand, the inherent intermittent cutting characteristics of whirl milling can easily induce destructive regenerative chatter in highly dynamic machining. This unstable vibration will not only drastically deteriorate the surface integrity of the parts, but also pose a serious safety threat to cutting tools and machine tools [4]. In the early days, parameter selection mostly relies on process manuals and trial cutting methods, which are costly and make it difficult to ensure the optimality of the solution. Although the subsequently developed intelligent

*Corresponding author: lixiaonan.li@outlook.com
[a]orcid.org/0009-0002-5708-8480; [b]orcid.org/0009-0006-5322-945X
DOI: http://dx.doi.org/10.17515/resm2026-2080im0730rs

optimization algorithms can handle multi-objective problems, they often simplify complex vibration control into compromising soft indicators, which can easily lead to instability risks in actual engineering [5]. Integrating artificial intelligence into the industrial manufacturing process more deeply to solve such optimization problems of multi-physics coupling is the key to realizing the transformation from Industry 4.0 to the more resilient and intelligent Industry 5.0 [6]. Therefore, how to construct a multi-objective parameter optimization scheme that can take chatter stability as a hard physical constraint and collaboratively optimize processing efficiency and quality under this premise has become an urgent problem to be solved in the field of whirl milling technology.

Optimizing whirl milling parameters is key to improving part performance. Current research focuses on building an optimization framework, improving solution algorithms and precision tool design to achieve coordinated control of processing quality and efficiency. Guo et al. proposed an improved method based on the analytic hierarchy process to address the problem of lack of comprehensive quantitative indicators in the surface integrity evaluation of large screws. The results showed that the evaluation model constructed by it improved the surface integrity by 64% compared with the original processing parameters of the factory, verifying the effectiveness of the proposed strategy in comprehensive evaluation and optimization [7]. To address the challenge of selecting milling parameters for irregular sheet metal parts, Chen et al. developed a multi-objective optimization framework that balanced efficiency with the quality of side-face machining. The results indicated that both the coupled model and the improved algorithm demonstrated good effectiveness in the multi-objective optimization of milling irregular sheet metal parts [8]. Yu et al. found that the profile design of hard cyclone tools used to process ZC1 worms had the risk of overcutting, and therefore proposed a design and verification method based on precision tool profiles. The results indicated the proposed tool design method could avoid overcutting effectively, and the maximum contour error was less than 3 μm under different cutting parameters, which provided important value for the design of complex envelope processing tools [9].

Multi-Objective Gray Wolf Optimizer (MOGWO) has become a research hotspot for solving complex parameter optimization problems in the fields of manufacturing systems and material processing due to its excellent global search and convergence performance. Kumar G et al. proposed an optimal configuration design method based on MOGWO to address the complex and multi-objective problem of configuration selection for reconfigurable manufacturing systems. The results showed that MOGWO could obtain a series of non-dominated solutions, which provided a key basis for decision-makers to select appropriate manufacturing system configurations according to market demand [10]. Ekanem I et al. introduced the MOGWO algorithm to collaboratively optimize structural stability, lattice parameters, phase transition and other characteristics to solve the problem that traditional algorithms were difficult to deal with the multi-objective characteristics of crystal structures. The results showed this algorithm was superior to the traditional algorithm in terms of convergence speed, accuracy and solution quality, and could efficiently realize the analysis and classification of crystal structures [11]. Gopi T et al. proposed a hybrid optimization method that combined principal component analysis and MOGWO for the multi-objective optimization problem of AA2014 aluminum alloy turning. The results showed that the proposed hybrid method could obtain a better combination of processing parameters in a very short calculation time, showing great potential for application in manufacturing [12].

In summary, existing research mostly focuses on the multi-objective performance trade-off or independent chatter stability analysis of whirl milling, but has not yet formed a systematic optimization solution that deeply integrates the two. Without hard constraints based on physical mechanisms, simple intelligent algorithm optimization can easily recommend high-risk pseudo-optimal solutions, while independent stability analysis cannot take into account both processing efficiency and quality. Therefore, this study constructs a parameter optimization scheme that combines the hard constraints of chatter stability and the Improved Multi-Objective Gray Wolf Optimizer (IMOGWO), to provide the best solution found under the specified parameters and computational conditions. The innovation of the research lies in converting the flutter physical model into nonlinear hard constraints, which delimits the safety boundary for parameter optimization. The research designs the IMOGWO algorithm that integrates Tent chaotic mapping

and adaptive penalty mechanism, and improves the global search efficiency and convergence performance by internalizing the physical constraints into the algorithm's screening mechanism. This solution realizes the deep integration of physical constraints and intelligent optimization, and provides a new paradigm of parameter optimization that considers safety and performance for highly dynamic processing.

2. Methodology

To solve the problem of ignoring the risk of chatter instability in whirl milling parameter optimization, an optimization scheme integrating physical constraints is proposed. This solution first builds a multi-objective optimization model containing hard constraints on flutter stability. Then, it designs IMOGWO for solution, improves global search capabilities by integrating Tent chaotic mapping, and uses an adaptive penalty function to internalize physical constraints into the screening mechanism of the algorithm.

2.1 Development of A Multi-Objective Optimization Scheme Incorporating Flutter Constraints

2.1.1 Development of A Multi-Objective Performance Function for Whirl Milling

The core of whirl milling parameter optimization is to consider machining efficiency and quality, and avoid unstable chatter in highly dynamic processes [13-14]. However, existing methods are limited to static frames. Due to the lack of consideration of the physical constraints of regenerative flutter, its optimization results often fail because of instability [15]. Accordingly, the study introduces dynamic flutter stability constraints into the multi-objective optimization system. Under the framework, it's necessary to clarify the performance optimization goals. The study uses material removal rate and surface roughness to quantify processing efficiency and quality, where the material removal rate is shown in Equation (1) [16].

$$MRR = (f_z \cdot N_t \cdot n) \cdot a_p \cdot a_e \tag{1}$$

In Equation (1), MRR is the material removal rate, n is the spindle speed, f_z is the feed per tooth, a_p and a_e represent the axial and radial cutting depths respectively, and N_t is the number of teeth on the cutting tool. The expression of surface roughness R_a is shown in (2) [17].

$$R_a = C_{Ra} \cdot n^{\lambda_1} \cdot f_z^{\lambda_2} \cdot a_p^{\lambda_3} \tag{2}$$

In Equation (2), C_{Ra}, λ_1, λ_2, and λ_3 are all empirical coefficients obtained by fitting experimental data. The specific values of each empirical coefficient are: C_{Ra}=2.76, λ_1=-0.214, λ_2=0.628, λ_3=0.173. This model is based on the TC4 titanium alloy ball screw rotary milling single factor experimental dataset, with a total of 36 sets of effective process roughness samples collected, and coefficient fitting completed using multivariate nonlinear least squares method. The coverage range of experimental parameters is the effective applicable range of the model: the spindle speed n is 1200-2400r/min, the feed rate f_z per tooth is 0.04-0.12mm/z, and the axial cutting depth a_p is 0.2-0.6mm. Beyond this range, the model prediction error will significantly increase. The coefficient of determination for the goodness of fit of the model is R^2=0.942, and the root mean square error is 0.227 μ m. The study reserves 8 sets of test samples for model validation, with an average relative prediction error of 7.8% in the test set. Due to random factors such as tool wear and small vibrations during workpiece clamping, the model has inherent uncertainty, and the maximum deviation in predicting roughness does not exceed $\pm$ 0.35 μ m. The subsequent parameter optimization of this study is all constrained within the above experimental parameter range to ensure the reliability of the roughness objective function prediction and reduce the interference of model uncertainty on the Pareto front. After clarifying the performance optimization goals, the key to building this framework is how to transform the physical concept of flutter stability into executable mathematical hard constraints. The evolutionary relationship of this model structure is shown in Figure 1.

In Figure 1, the traditional path only includes static performance prediction, while the proposed framework incorporates a parallel dynamic flutter analysis module. This new module is used to

generate hard constraints on flutter stability, ensuring that the final optimization model can jointly handle the two dimensions of performance and safety.

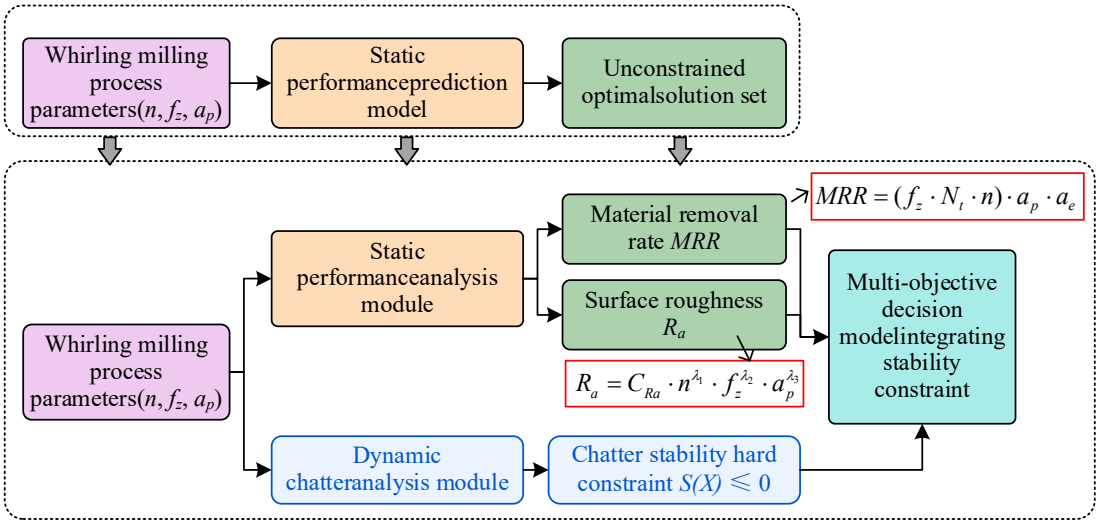


Fig. 1. Evolutionary diagram of the whirling milling multi-objective optimization model structure

2.1.2 Mathematical Transformation of Hard Constraints on Flutter Stability

The construction of the stability hard-constraint model starts from the physical description of the vibration behavior of the whirl milling processing system. The vibration in this process can be approximately expressed by a single degree of freedom dynamic equation, as shown in Equation (3).

$$m_{eq}\ddot{y}(t) + c_{eq}\dot{y}(t) + k_{eq}y(t) = F_{dyn}(t) \tag{3}$$

In Equation (3), $y(t)$ is the relative vibration displacement of the whirl milling processing system, $\dot{y}(t)$ and $\ddot{y}(t)$ represent the vibration speed and acceleration of the system respectively, where the variable t is the physical time. m_{eq}, c_{eq} and k_{eq} are equivalent modal mass, damping and stiffness, respectively. $F_{dyn}(t)$ is the dynamic cutting force. In the regenerative chatter problem of whirl milling, the dynamic cutting force$F_{dyn}(t)$ mainly originates from the regenerative effect between the cutter teeth, and its expression is shown in Equation (4).

$$F_{dyn}(t) = K_f \cdot a_p \cdot [y(t-\tau) - y(t)] \tag{4}$$

In Equation (4), K_f is the cutting force coefficient, and τ is the cutting time delay caused by the periodic cutting of the cutter teeth. $y(t-\tau)$ is the vibration displacement at the delay time. The size of τ is directly related to the process parameters, and its expression is shown in Equation (5).

$$\tau = \frac{60}{n \cdot N_t} \tag{5}$$

Equation (5) clarifies the quantitative mapping relationship between cutting time delay and spindle speed. By substituting equations (4) and (5) into equation (3), a complete time-delay differential equation describing the dynamic process of the whirl milling system can be constructed. However, it is extremely difficult to solve the stability bounds of this equation directly in the time domain. Accordingly, the study uses frequency domain analysis methods to establish a transfer function that can characterize the dynamic response characteristics of the system, as shown in Equation (6).

$$G(j\omega) = \frac{1}{k_{eq} - m_{eq}\omega^2 + jc_{eq}\omega} \tag{6}$$

In Equation (6), ω is the vibration angular frequency, and j is the imaginary unit. The stability of the whirl milling processing system is determined by the solution of the frequency domain characteristic equation, and its critical condition is closely related to the real part of the transfer function $G(j\omega)$. For the complete derivation process and assumptions of the expression from the

delay differential equation to the ultimate cutting depth, the Laplace transform is first applied to the single degree of freedom delay differential equation in equation (3) to obtain the system transfer function under zero initial conditions, as shown in equation (7).

$$G(s) = 1/[m(s^2 + 2\zeta\omega_n s + \omega_n^2)] \tag{7}$$

In equation (7), m is the equivalent modal mass of the system, ζ is the damping ratio of the system, ω_n is the natural angular frequency of the system, and s is the Laplace operator. The expression of s is shown in equation (8).

$$s = j\omega_c \tag{8}$$

In equation (8), ω_c is the critical flutter angular frequency. By substituting equation (8) into equation (7), the frequency domain transfer function $G(j\omega_c)$ can be obtained, and its partial expression is shown in equation (9).

$$Re[G(j\omega_c)] = (1-k)/(m[(1-k)^2 + (2\zeta k)^2]) \tag{9}$$

In equation (9), $k = (\omega_c/\omega_n)^2$ is the frequency ratio, and Re[·] represents the real part of the transfer function. The derivation of stability criteria relies on the following assumptions:

- The cutting process is a linear small amplitude vibration, and the dynamic cutting force is linearly related to the change in cutting thickness.
- The regeneration effect is the only triggering mechanism for flutter, ignoring other types of flutter such as modal coupling.
- The cutting force coefficient is considered a constant within the cutting parameter range of this study. Based on the above assumptions, the expression of dynamic cutting force is shown in equation (10).

$$F_d(t) = K_t b[y(t) - y(t-\tau)] \tag{10}$$

In equation (10), K_t is the tangential cutting force coefficient, b represents the cutting depth, and $y(t)$ is the current vibration displacement of the system. The study substitutes equation (10) into the dynamic equation and conducts frequency domain analysis to obtain the system characteristic equation, as shown in equation (11).

$$1 + K_t b[1 - e^{-j\omega_c\tau}]G(j\omega_c) = 0 \tag{11}$$

In equation (11), $e^{-j\omega_c\tau}$ is the complex exponential term corresponding to the delay. Setting the imaginary part of the characteristic equation to zero yields the relationship satisfied by the critical frequency, which is expressed as equation (12).

$$sin(\omega_c\tau) = 2\zeta k/(1-k) \tag{12}$$

In equation (12), under the given modal parameters and regeneration delay τ, the critical angular frequency ω_c of flutter can be obtained by numerical solution. Then, the real part of the characteristic equation is set to zero, and the expression for the ultimate cutting depth $a_{lim}(n)$ is obtained after sorting, as shown in equation (13).

$$a_{lim}(n) = \frac{1}{-2K_f \cdot min(Re[G(j\omega_c)])} \tag{13}$$

The reason why only the real part of the transfer function is used to determine the stability criterion here is that the imaginary part condition of the characteristic equation has been used to solve and determine the critical flutter frequency ω_c. At this specific critical frequency, the stability of the system is only determined by the real part condition of the transfer function. Therefore, the ultimate cutting depth can be directly calculated using the real part of the transfer function at point ω_c. The cutting force coefficient K_t, in the form of a linear proportional term, is located at the denominator of the formula and directly determines the absolute position of the stability boundary. The regeneration delay τ is involved in the construction of the characteristic equation through the complex exponential term $e^{-j\omega_c\tau}$, and the solution result of the critical angular frequency ω_c is changed by the imaginary part constraint of equation (12), indirectly changing the value of $Re[G(j\omega_c)]$ and ultimately affecting the ultimate cutting depth. Given the modal parameters,

cutting force coefficient, and regeneration delay, the stability blade diagram corresponding to equation (13) can be reproduced by relying on the entire derivation process described above.

To facilitate the unified calling of subsequent algorithms, the set of process parameters to be optimized is defined as a three-dimensional column vector $X = [n, f_z, a_p]^T$. From this, the complex dynamics problem can be converted into a simple stability hard constraint function $S(X)$, as shown in Equation (14).

$$S(X) = a_p - a_{lim}(n) \tag{14}$$

In Equation (14), when $S(X) \leq 0$, it means the machining process under the current parameter vector X is in a stable state. Equation (3) is the single degree of freedom time-delay dynamic differential equation of the rotary milling system, which is the physical origin equation describing the evolution of the system's vibration displacement over time. The current stability hard constraint function is equation (14). The intrinsic relationship between the two is as follows: based on equation (3), the regenerative dynamic cutting force (equation (4)) and the time delay formula (equation (5)) are introduced, and the transfer function (equations (6)-(9)) is obtained through Laplace transform and frequency domain analysis. Based on the stability assumption, the ultimate cutting depth is derived (equation (13)). It substitutes the optimized process parameter vector into the limit cutting depth criterion for differential calculation and mathematical encapsulation, and obtains the stability hard constraint function equation (14) that can be called by the IMOGWO algorithm. In short, equation (3) provides the physical mechanism of flutter, which is transformed into equation (14) for algorithm discrimination of inequality constraints through time delay modeling and frequency-domain stability derivation.

This study uses a single degree of freedom dynamic equation to describe the vibration behavior of a rotary milling system. Here, the applicable prerequisites of the model are explained. The research object of this article is the TC4 titanium alloy ball screw rotary milling machining condition. The stiffness of the workpiece system is significantly lower than that of the tool system, and the radial direction of the workpiece is the dominant vibration direction during the machining process. Therefore, $y(t)$ in equation (3) represents the radial vibration displacement of the workpiece. The modal response amplitude of the tool body is relatively low, and the influence of high-order modal coupling can be ignored. Using a single degree of freedom model can characterize the main vibration behavior of the system. Rotary milling is characterized by multi cutting engagement, intermittent cutting, and dynamic contact state variations. To account for these features, the tool geometric parameters and tooth number N_t are directly incorporated into the time-delay calculation and the material removal rate objective function. Intermittent cutting can produce amplitude modulation effects on dynamic cutting forces, and in this study, the regenerative effect remains the dominant cause of chatter. The directional cutting force coefficient is coupled to the frequency domain transfer function solving process and participates in the calculation of the ultimate cutting depth. Meanwhile, it should be noted that if the tool and workpiece stiffness levels are close and there is a significant multimodal coupling phenomenon, the single degree of freedom model is no longer applicable.

The delay term $\tau = \frac{60}{n \cdot N_t}$ in the text corresponds to the tooth passage period, and this expression does not directly copy the delay formula of ordinary milling. Rotary milling has a special relative motion relationship between the tool and the workpiece. The workpiece rotates at high speed, and the tool performs feed motion. Adjacent teeth scan the machined surface of the workpiece in sequence, and the regenerated vibration pattern is generated by the superposition of the cutting trajectories of the front and rear teeth. Regarding the research conditions of ball screw rotary milling in this article, the actual effective regeneration delay is consistent with the tool tooth passing cycle. However, there is a clear applicable boundary for this delay expression: when the cutting teeth frequently detach from the workpiece and the proportion of intermittent cutting contact is too high, the delay assumption will deviate. In this scenario, a time-varying delay model needs to be constructed for further analysis.

In the constructed dynamic model, the time delay effect is achieved by the delayed displacement term $y(t - \tau)$ within the dynamic cutting force in equation (4). It is used to characterize the

modulation effect of the residual vibration pattern on the workpiece surface caused by the previous tooth cutting on the current tooth cutting force, completing the mathematical expression of the regenerative chatter effect. For the intermittent cutting effect, this article does not explicitly construct the time-varying cutting force coefficient, but defines it as the applicable condition of the model: Within the parameter range studied in this article, the effective contact between the cutting teeth and the workpiece has a high proportion, and intermittent cutting mainly changes the amplitude of the cutting force, without changing the regenerative induction mechanism of chatter. Therefore, the above-mentioned time delay form can be used. If the degree of intermittent cutting significantly increases, it is necessary to introduce time-varying coefficients corresponding to intermittent cutting to further modify the model. The constraint function is solved from the physical dynamics model through middle-level theory, and finally the complete logical framework of the hard constraint is extracted at the application layer, as shown in Figure 2.

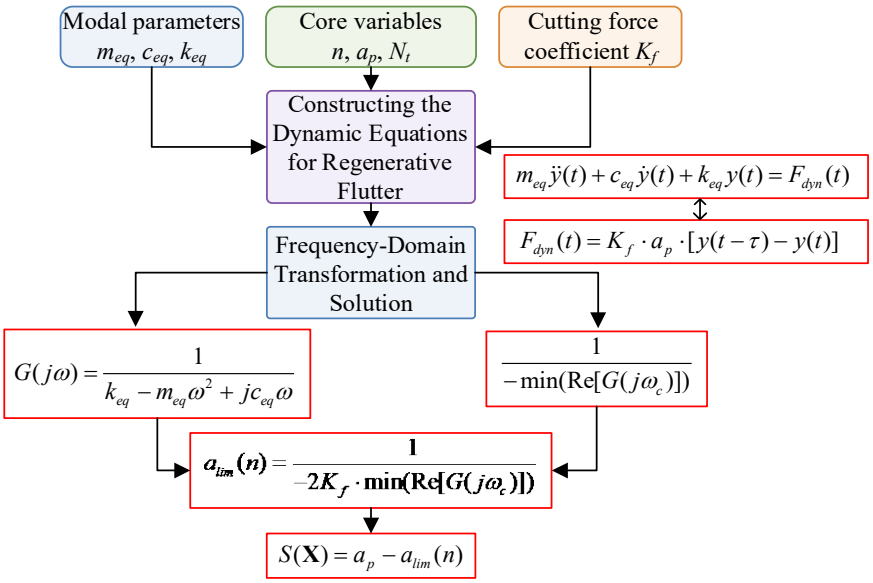


Fig. 2. Logical framework diagram for generating vibration stability constraints

Figure 2 illustrates the derivation framework from physical inputs to mathematical constraints. The dynamic parameters m_{eq}=12.5kg, c_{eq}=750N·s/m, k_{eq}=1.5 × 107N/m in this study are taken from the measured results of the hammer impact modal test of TC4 titanium alloy ball screw workpiece. The dynamic parameters characterize the radial first-order dominant mode of the workpiece under rotary milling, corresponding to the workpiece side mode of the machine tool tool workpiece system. The experiment uses a force hammer excitation combined with an acceleration sensor to collect the radial vibration response of the workpiece and obtain the frequency response function. The least squares complex frequency domain method is used to identify the modal parameters mentioned above. The cutting force coefficient K_f = 850MPa is derived from the TC4 titanium alloy multi group rotary milling single factor cutting test dataset, and is obtained through regression fitting using the least squares method based on a linear cutting force model. The empirical coefficients used in the surface roughness objective function in the article are also based on the sample dataset of the rotary milling experiment in this study, and are fitted using the least squares regression method. The natural angular frequency of the system is calculated by the equivalent mass and equivalent stiffness, and its expression is shown in equation (15).

$$\begin{cases}\omega_n=\sqrt{k_{eq}/m_{eq}}\\ f_n=\omega_n/(2\pi)\end{cases} \tag{15}$$

In equation (15), f_n is the natural frequency. By using the natural angular frequency ω_n of the system, the natural frequency f_n can be converted. By substituting the parameters, the natural frequency can be calculated to be approximately 174 Hz. Due to the softening effect of cutting stiffness and damping changes during the cutting process, the actual vibration frequency will shift relative to the natural frequency of the structure. The calculated natural frequency of

approximately 174 Hz represents the structural natural frequency obtained from the equivalent mass and stiffness parameters. It should be distinguished from the higher-frequency vibration components observed in the simulated frequency-domain response. The vibration response may contain frequency components associated with the periodic cutting excitation, tooth-passing effects, regenerative dynamics, and other dynamic responses of the intermittent whirl-milling process. Therefore, the frequency-domain peak observed in the simulation should not be directly identified as the structural natural frequency solely on the basis of its spectral location. This study has completed the verification of all physical quantities, with equivalent mass unit N·s/m, equivalent damping unit N/m, equivalent stiffness unit N/m, and cutting force coefficient unit MPa. The dimensions of each physical quantity are self-consistent and can be directly substituted into the dynamic equations to complete simulation calculations.

By integrating static performance dimensions with this strict flutter constraint, the study ultimately develops a multi-objective optimization model that simultaneously optimizes the efficiency, quality, and stability of whirl milling, as shown in Equation (16).

$$\begin{cases} min\, F(X) = [-MRR(X), R_a(X)]^T \\ \quad subject\ to \quad S(X) \le 0 \\ \quad X \in [X_{min}, X_{max}] \end{cases} \tag{16}$$

In Equation (16), $F(X)$ is the multi-objective function vector to be optimized, $-MRR(X)$ and $R_a(X)$ represent the material removal rate and surface roughness sub-objective functions respectively, T represents the vector transpose, and $X \in [X_{min}, X_{max}]$ defines the value boundary of the process parameters. In summary, the study finally forms a constrained multi-objective optimization model by constructing a static performance evaluation dimension that includes efficiency and quality, and integrating dynamic stability hard constraints derived layer by layer based on the flutter mechanism. The establishment of this model lays a solid foundation for the subsequent improvement of optimization algorithms to efficiently solve such complex constraint problems.

2.2 Design of The IMOGWO Algorithm Optimized for Whirl Milling

2.2.1 Population Initialization and Update Mechanisms of The MOGWO Algorithm

The constrained multi-objective optimization model constructed in this study has the characteristics of high dimensionality, multi-objectives and strong non-linear constraints. If the traditional enumeration method is used to traverse all parameter combinations, the calculation cost is extremely high. Therefore, the study introduces MOGWO as the basic solving framework. This algorithm simulates the cooperative hunting behavior of wolves. Its core is the vector pulling process in which the alpha wolf guides the group to update its position, as shown in Figure 3.

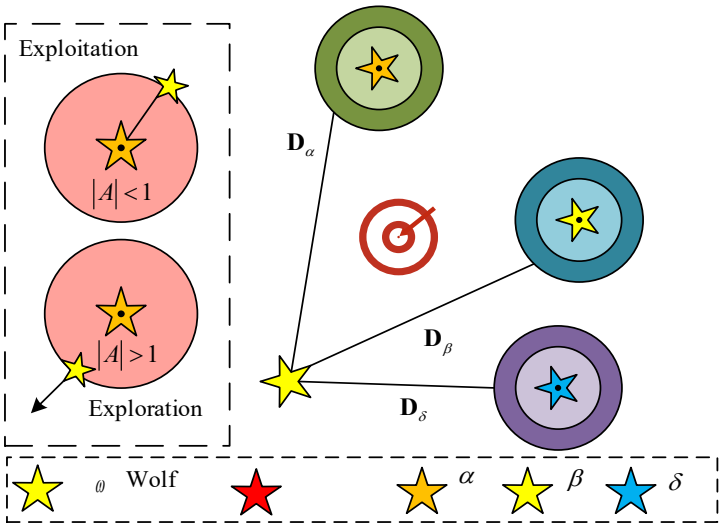


Fig. 3. Topological diagram of position update vectors for the gray wolf population in multi-objective optimization

In Figure 3, the position update of the ordinary parameter solution (ω wolf) is pulled by the weighted vector of the current optimal solution guidance set (α, β, and δ wolf) and converges towards the Pareto optimal direction. The first step in the guidance process is to calculate the surrounding distance vector between the current ordinary wolf and the three alpha wolves, whose expression is shown in Equation (17) [18].

$$\begin{cases} D_\alpha = |C_1 \cdot X_\alpha(g) - X(g)| \\ D_\beta = |C_2 \cdot X_\beta(g) - X(g)| \\ D_\delta = |C_3 \cdot X_\delta(g) - X(g)| \end{cases} \tag{17}$$

In Equation (17), g is the current iteration number of the algorithm, $X(g)$ is the position vector of the ordinary wolves. $X_\alpha(g)$, $X_\beta(g)$, and $X_\beta(g)$ are the position vectors of the three alpha wolves, respectively. C_1, C_2, and C_3 are the coefficient vectors. Using Equation (17), the step vectors toward the three alpha wolves can be further derived, and the next-generation positions of the ordinary wolves can ultimately be determined. The calculation process is shown in Equation (18).

$$\begin{cases} X_1 = X_\alpha(g) - A_1 \cdot D_\alpha \\ X_2 = X_\beta(g) - A_2 \cdot D_\beta \\ X_3 = X_\delta(g) - A_3 \cdot D_\delta \\ X(g+1) = \dfrac{X_1 + X_2 + X_3}{3} \end{cases} \tag{18}$$

In Equation (18), A_1, A_2, and A_3 are coefficient vectors.

2.2.2 Improvements to Population Initialization Based on Chaotic Mappings

Although the collaborative update mechanism guided by the alpha wolf of the standard MOGWO algorithm can balance the exploration and development capabilities of the algorithm effectively, its optimal performance relies heavily on the distribution quality of the initial population. The traditional random initialization method is difficult to ensure uniform coverage of the population in the solution space, and can easily cause the algorithm to converge prematurely or fall into local optimality [19-20]. Therefore, the study introduces Tent chaotic mapping to improve the population initialization process, using the ergodicity and pseudo-randomness of the chaotic sequence to evenly distribute the initial wolf population in the solution space and improve the search diversity in the early stage of the algorithm, as shown in Equation (19).

$$z_{s+1} = \begin{cases} 2z_s, & 0 \le z_s < 0.5 \\ 2(1 - z_s), & 0.5 \le z_s \le 1 \end{cases} \tag{19}$$

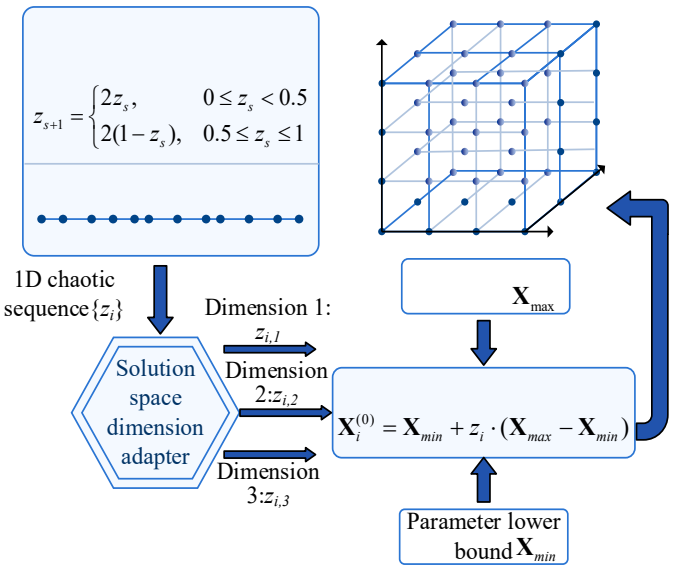


Fig. 4. Block diagram of the initial population generation mechanism based on the Tent chaotic mapping

In Equation (19), z_s is the sth value in the chaotic sequence. Using this chaotic sequence, the initial population can be evenly mapped to the entire parameter solution space. The specific initialization process is shown in Equation (20).

$$X_i^{(0)} = X_{min} + z_i \cdot (X_{max} - X_{min}) \tag{20}$$

In Equation (20), $X_i^{(0)}$ represents the initial parameter vector of the ith gray wolf individual. This improved mechanism, which replaces the traditional random number generator with a chaotic mapping engine, is illustrated in Figure 4.

In Figure 4, after the chaotic sequence is mapped through the solution space, it can ensure that the initial population achieves uniform coverage in the parameter space, laying a solid foundation for the global search of the algorithm.

2.2.3 Adaptive Penalty Mechanism Incorporating Stability Constraints

To further address the fundamental issue of the lack of constraints in the standard position update mechanism, the study designs an adaptive penalty function that incorporates stability constraints. This function quantifies the degree of constraint violation by defining a penalty term $P(X)$, as shown in Equation (21).

$$P(X) = M \cdot max(0, S(X)) \tag{21}$$

In Equation (21), M is a very large positive number, and the $P(X)$ penalty term is incorporated into the algorithm's fitness evaluation. In multi-objective optimization, algorithms rely on the Pareto non-dominance ordering to compare the relative merits of solutions, using an evaluation vector containing the values of each objective as the primary basis for comparison. By applying penalty terms to all target dimensions, the study constructs the evaluation vector $F_{penalized}(X)$, which is ultimately used for Pareto non-dominance ranking, as shown in Equation (22).

$$F_{penalized}(X) = [-MRR(X) + P(X), R_a(X) + P(X)]^T \tag{22}$$

By imposing an extreme penalty on solutions that violate constraints through Equation (22), the study successfully internalizes the hard constraints of chatter at the physical level into the screening mechanism of the algorithm, ensuring that the final output whirl milling parameter combinations are all within the safe machining boundary.

Hard constraints represent the physical boundary conditions that must be strictly satisfied for optimizing the output solution, and solutions that do not meet these conditions are considered infeasible solutions that cannot be adopted in engineering. The flutter hard constraint in this study means that the final output process parameters must meet $S(X) \leq 0$. Constraint processing based on penalty functions is an indirect constraint method, which does not directly delete infeasible individuals in the iterative population, but reduces their evolutionary selection competitiveness by deteriorating the infeasible solution objective function.

This study adopts a mixed constraint strategy of penalty function sorting and Pareto archive secondary strict screening. The complete and reproducible penalty function calculation process is as follows:

- It inputs the process parameter vector X, substitutes it into equation (21) to obtain the stability constraint value $S(X)$.
- If $S(X) \leq 0$ (stable feasible solution), the penalty term $P = 0$. If $S(X) > 0$ (unstable and infeasible solution), penalty term $P = M \cdot S(X)$.
- It overlays the penalty term P onto two original objective functions, and uses the modified objective for Pareto sorting within the population.
- It performs a second check when updating external Pareto files in each generation, directly removing all unstable solutions of $S(X) > 0$ in the file.

After point-by-point verification of the final Pareto archive, all retained solution sets meet the criteria of $S(X) \leq 0$, and there are no unstable process solutions in the archive. The iterative stage retains infeasible individuals to participate in the search, with the aim of maintaining population diversity and avoiding premature convergence of the algorithm. The study finally constructs the

IMOGWO algorithm by integrating the Tent chaotic mapping initialization strategy and the adaptive penalty mechanism integrating stability constraints. Figure 5 illustrates the overall structure of the algorithm.

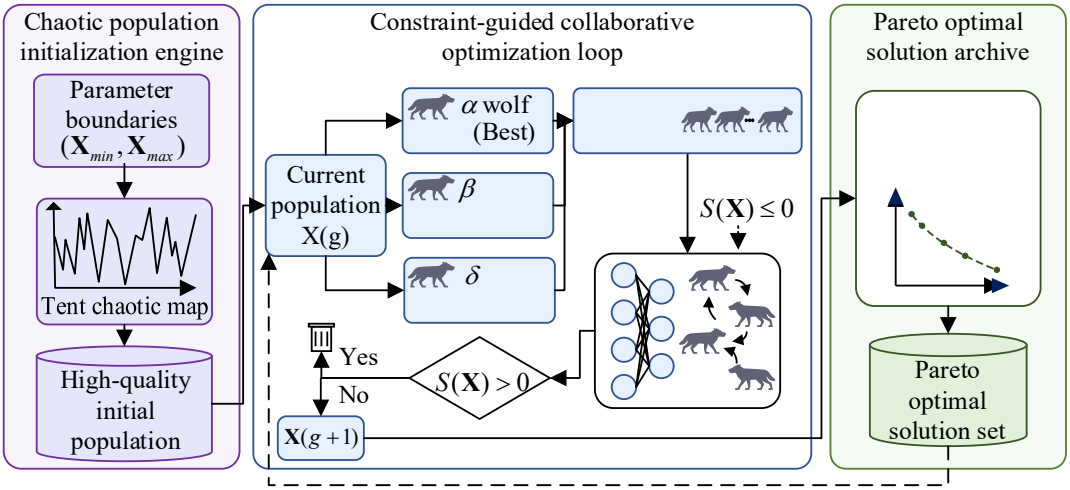


Fig. 5. Structural flowchart of the improved multi-objective gray wolf algorithm

In Figure 5, high-quality initial population generated by the chaos initialization engine is injected into the constraint-guided collaborative optimization loop. In each iteration, effective solutions that pass the stability check are sent to the Pareto optimal solution archive for update, and the optimal solutions in the archive will feed back to guide the evolution of the next generation population, forming a complete closed-loop information flow. In summary, the study combines the constructed multi-objective physical model integrating chatter stability with the IMOGWO solution algorithm, and finally forms a set of closed-loop solutions from the definition of the whirl milling problem to the optimization of processing parameters. The overall technical framework of the program is shown in Figure 6.

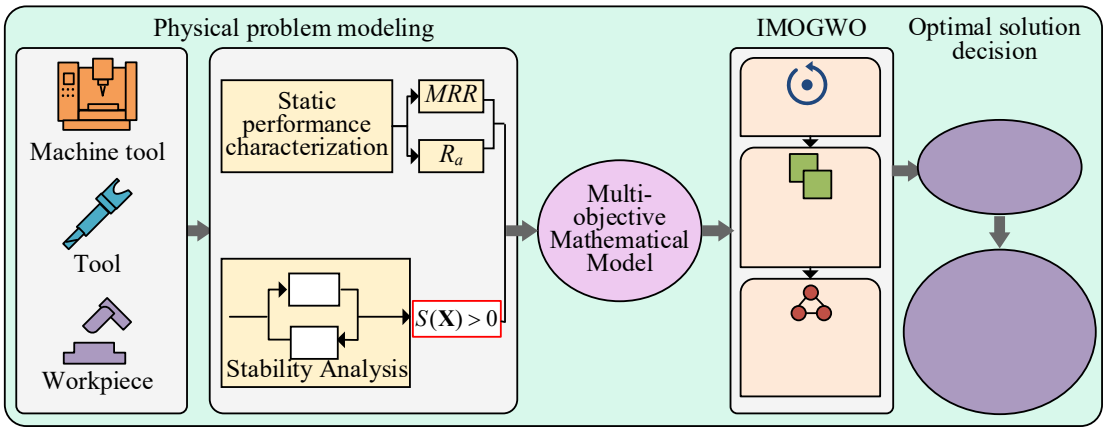


Fig. 6. Overall technical framework of the whirl milling parameter optimization method

In Figure 6, the physical problem modeling stage realizes the transformation from physical entities to digitally constrained multi-objective mathematical models. As an intelligent optimization engine, the IMOGWO stage integrates three major mechanisms: chaos initialization, constraint isolation and core optimization. Finally, the optimal solution optimization stage is responsible for weighing the Pareto optimal front output from the engine and outputting a specific set of optimal process parameters that can be directly applied in the form of a recommended solution. In summary, by constructing an optimization model that incorporates hard constraints on chatter stability, and designing the IMOGWO algorithm that integrates chaotic initialization and adaptive penalty mechanisms to solve it, the study finally obtains a set of optimal process parameters for whirl milling that takes into account high stability, high efficiency and high quality.

3. Results and Analysis

To validate the effectiveness of the constrained multi-objective optimization model, the optimization results with and without constraints were compared in multiple dimensions. Subsequently, to prove the advantage of the IMOGWO algorithm, a comprehensive performance evaluation was conducted with three mainstream algorithms such as MOGWO and Non-dominated Sorting Genetic Algorithm-II (NSGA-II) in terms of search quality, quantitative indicators and convergence speed, and finally verified the advancement and robustness of the proposed scheme.

3.1 Development and Configuration of a Simulation Verification Platform for TC4 Titanium Alloy Ball Screws

To systematically verify the accuracy of the constructed constrained multi-objective optimization model and the optimization superiority of IMOGWO, the whirl milling process of a typical TC4 titanium alloy ball screw in the aerospace field was selected as an engineering verification example. All simulation calculations were based on physical models constructed through research, and parameters were set based on public literature and authorized industrial processing measurement experience. The simulation relied on the algorithm population and iterative mechanism to complete adaptive iterative optimization within the complete parameter interval, to carry out model verification and comparative analysis of algorithm performance. The detailed parameter configurations of all compared algorithms are listed in Table 1.

Table 1. Experimental simulation environment and key parameter configuration

Category	Item	Configuration
Hardware Environment	Operating system	Windows 10 Pro
	CPU	Intel Core i9-13900K @ 3.00GHz
	RAM	32GB
Software Environment	Simulation Platform	MATLAB R2023a
Optimization Parameter Boundaries	n (r/min)	[1000, 3000]
	f_z (mm/z)	[0.02, 0.10]
	a_p (mm)	[0.2, 1.5]
Physical Model Parameters	Workpiece Material	TC4 Titanium Alloy
	Tool Type	Carbide Whirling Cutter
	m_{eq} (kg)	12.5
	c_{eq} (N·s/m)	750
	k_{eq} (N/m)	1.5×107
	K_f (MPa)	850
	N_t	6
Algorithm Parameters	Optimization Algorithm	IMOGWO
	Population size	100
	Max iterations	500
	Pareto archive size	100
	Chaotic mapping strategy	Tent map
	M	1.0×109

Regarding the randomness of multi-objective optimization algorithms, the performance statistics and convergence analysis of all algorithms in this study are based on the results of 20 independent repeated runs. We have set the stopping criteria for the algorithm to reach the maximum objective function evaluation budget limit (40000 calls, corresponding to a population size of 80 and a maximum iteration count of 500 generations). The initial condition of the algorithm was the random initialization of the population. To eliminate the uncertainty of random initialization and ensure 100% algorithm repeatability, we have uniformly set a fixed random seed (Random Seed=42) in all independently run simulation scripts, which has been noted in the supplementary code file. All multi-objective comparison algorithms in this study adopted a unified fair comparison

condition, with a population size set to 80 individuals. The evaluation process, process parameter search space, IGD, and HV index calculation rules were all kept consistent.

Simple iterative algebra could not directly and equivalently measure the computational efficiency of algorithms. In this paper, the total evaluation times of the objective function were used as the evaluation basis for efficiency comparison. This indicator calculated the total number of times the algorithm called the performance/constraint model, and was a universal standard for measuring computational costs in the field of multi-objective optimization.

3.2 Validation of The Flutter Stability Constraint Model and Analysis of Dynamic Responses

To demonstrate the rationality of the penalty coefficient M=109, sensitivity comparison tests were conducted with M=105, M=107, M=109, and M=1011, using a population size of 80 and 150 iterations. The test results are shown in Table 2.

Table 2. Comparison of algorithm performance under different penalty coefficients

Penalty coefficient	The number of unstable solutions mixed in the file	The number of feasible Pareto solutions
10^5	12	21
10^7	2	34
10^9	0	36
10^{11}	0	17

According to Table 2, the distribution of solution sets and objective function intervals for the two feasible Pareto frontiers with $M=10^7$ and $M=10^9$ were basically consistent. When $M=10^9$, both zero instability solutions of the archive and a sufficient quantity of feasible solutions were retained. This indicated that the optimization results were stable within a reasonable parameter range, and the Pareto front obtained in this paper was not an artificial result caused by the selection of penalty coefficients. Based on the comprehensive constraint satisfaction ability and global optimization performance, this study ultimately selected $M=10^9$.

To verify the effectiveness of the constrained multi-objective optimization model constructed in this study, the multi-dimensional performance of the Pareto solution sets under the two schemes with stability constraints (solved by IMOGWO) and without constraints (solved by MOGWO) was compared. Figure 7 presents the results. In Figure 7(a), when no constraints were imposed, some of the high-performance solutions found by the algorithm were close to 1.0 in the machining efficiency dimension, but their machining stability index values dropped below 0.2, which was a physically infeasible unstable solution. From Figure 7(b), after applying hard constraints, the machining stability indicators of all solutions were strictly limited to a high range above 0.8. Among them, the optimal compromise solution could still achieve 0.82 and 0.90 in machining efficiency and surface quality indicators while ensuring the stability of 0.98.

To further investigate the consistency between the stability criteria constructed and the dynamic response results, this paper compares and analyzes the theoretical stability criteria with the vibration displacement response obtained from dynamic simulation. It should be clarified that this comparison belongs to internal consistency verification under the same dynamic modeling framework, rather than independent physical experiment verification. The theoretical stability criteria and dynamic simulation are based on the same system dynamics parameters, regeneration effect assumptions, and cutting force models. Therefore, this validation is mainly used to check whether there is a consistent trend and state discrimination result between the stability boundary criteria and the time-domain dynamic response, and cannot be used as proof of the independent experimental effectiveness of the model. Dynamic simulation adopts a sampling frequency of 20

kHz, with each operating condition simulated for 0.2 seconds, and the vibration displacement signal during the stable phase is extracted for analysis. The "energy" in the frequency domain results is represented by normalized relative amplitude and is only used to compare the relative strength of vibration response under different operating conditions, and does not represent the actual physical energy.

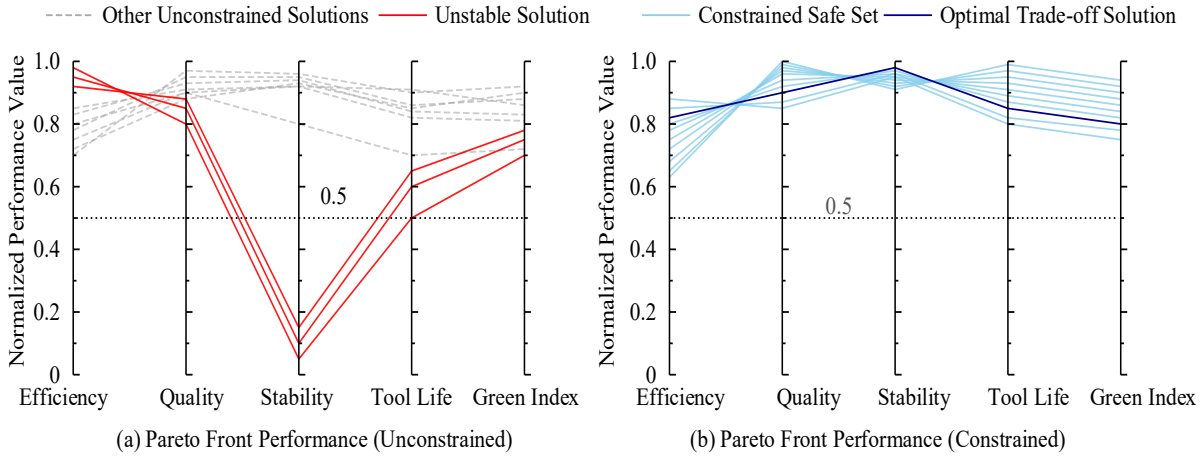


Fig. 7. Multidimensional performance comparison of Pareto solution sets with and without constraints

In the stability state change results shown in Figure 8 (a), when the spindle speed is 1800 r/min and the axial cutting depth increases from 1.5 mm to 2.0 mm, the stability criterion shifts from the stable region to the unstable region. In the dynamic simulation vibration amplitude results shown in Figure 8 (b), within the theoretically predicted unstable region, the vibration amplitude of the dynamic simulation significantly increases. Under typical working conditions of spindle speed of 1500 r/min and axial cutting depth of 2.5 mm, the simulated vibration amplitude reaches 4.11 mm, while the simulated vibration amplitude within the theoretically stable region remains below 0.30 mm.

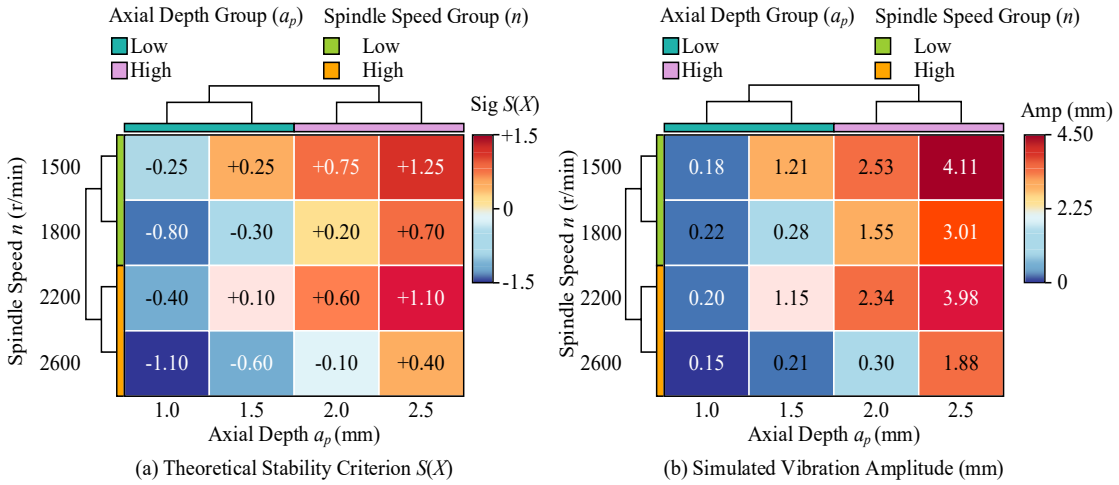


Fig. 8. Stability boundary verification for typical parameter points

In terms of dynamic simulation results, the simulation amplitude of 4.11 mm under unstable conditions was a typical single simulation output result, and the optimized Pareto solution set average vibration amplitude of 0.18 mm was obtained from the Pareto solution set statistics of 20 independent optimization runs. The amplitude fluctuation uncertainty range was 0.16-0.21 mm. It should be noted that the vibration amplitude was a constraint effectiveness verification indicator in this article, not an optimization objective function. The optimization algorithm itself did not directly minimize the vibration amplitude. The physical root of the amplitude reduction was that stability constraint $S(X) \leq 0$ restricted the process parameters within the flutter stability domain, avoiding the self-sustaining amplification effect of regenerative flutter, and the system only

retained forced vibrations with smaller amplitudes. The simulation comparison results showed that the constraint model constructed in this study could accurately distinguish the stable/unstable range of rotary milling processing, providing a reliable physical model basis for the stable screening of rotary milling process parameters.

To further evaluate the predictive accuracy of stability criterion $S(X) \leq 0$ within the entire optimization parameter domain, in addition to typical operating conditions, multiple combinations of different spindle speeds and axial cutting depths were selected, and dynamic simulation verification was carried out covering both the theoretically stable and unstable regions. A total of 10 combinations of spindle speed and axial cutting depth were selected, including 5 theoretically stable conditions and 5 theoretically unstable conditions. These conditions covered the main spindle-speed and axial-depth ranges considered in the optimization process and were selected to represent both sides of the theoretical stability boundary. Then, the study compared the theoretical prediction results of stability criteria with the simulated vibration amplitude state. When the simulated vibration amplitude was below 0.30 mm, it was classified as a stable cutting state, whereas when the simulated vibration amplitude was greater than 0.30 mm, it was classified as an unstable cutting state. The 0.30 mm threshold was adopted as a classification criterion for distinguishing the low-amplitude stable response from the high-amplitude response within the present dynamic simulation framework. It was not intended to represent a universal experimentally calibrated physical stability threshold. Therefore, the classification results based on this threshold should be interpreted within the specific dynamic model, parameter range, and simulation conditions investigated in this study.

The uncertainty of the present classification results was mainly associated with the limited number of validation conditions, the selected process-parameter combinations, and the assumptions and parameters of the underlying dynamic model. The 10 validation conditions were used to examine model consistency rather than to estimate a population-level classification accuracy. Although 20 independent optimization runs were conducted in the optimization study, the resulting amplitude fluctuation range of 0.16-0.21 mm describes the variation of the Pareto-solution vibration amplitude and is not a confidence interval for the 10 classification conditions in Table 3. Therefore, no experimentally based confidence interval was assigned to the 10-condition classification result. Since the theoretical stability criterion and the dynamic simulation responses were derived within the same underlying dynamic modeling framework, the validation data were not independent physical measurements. The resulting agreement was therefore used to assess the internal consistency between the theoretical criterion and the dynamic simulation response rather than to establish independent experimental classification accuracy. The comparison results of each working condition are shown in Table 3.

From Table 3, the theoretical stability criterion classifications were consistent with the corresponding dynamic simulation states for all 10 selected operating conditions, with no disagreement observed between the two model-derived results. This 10/10 agreement indicates that the stability criterion and the dynamic simulation response exhibit consistent state classification under the specified model assumptions and parameter range. However, because both the theoretical criterion and the dynamic simulation were established from the same underlying dynamic model and regenerative assumptions, this agreement should be interpreted as internal model-consistency evidence rather than independent experimental validation. Therefore, the results in Figure 8 and Table 3 do not establish the physical validity or engineering safety of the proposed stability criterion. Independent cutting experiments with measured vibration responses are required for further physical validation. It should be noted that this criterion was based on the assumption of a single degree of freedom model dominated by regenerative flutter. When significant multimodal coupling, severe tool wear, and strong time-varying intermittent cutting occurred in actual machining, prediction bias might occur.

To compare the machining process of typical optimal solutions with and without two constraints from the dynamic response level, the study selected two representative parameter points in Figure 8, namely the unstable working condition (n =1800r/min, a_p=2.0mm) and the stable working condition (n =1800r/min, a_p=1.5mm). Then, the study conducted a joint analysis of the simulated

vibration signal in the time-frequency domain. Figure 9 shows the results. In Figure 9(a), the vibration displacement of the Unconstrained Solution (US) increased from 0 to nearly 5.0 mm within 0.05 s, showing a typical exponential divergence trend. The corresponding frequency domain figure 9(c) shows that there was a sharp peak with extremely concentrated energy near 1500Hz, with an amplitude as high as 0.95, which was a clear characteristic of chatter instability. In Figure 9(b), the vibration displacement of the Constrained Solution (CS) obtained in the study converged quickly after the initial disturbance, and had decayed to less than 0.1mm after 0.03s. The corresponding energy distribution in Figure 9(d) was gentle without any abnormal peaks. Taken together, the constrained optimization model constructed in this study could guide the generation of processing parameters to avoid destructive chatter and solve the stability problem in highly dynamic whirl milling.

Table 3. Comparison of stability criterion theory prediction and dynamic simulation results

Serial number	spindle speed (r/min)	Axial cutting depth/mm	Theoretical criteria for predicting states	Simulate the actual state
1	1200	1.4	Stable	Stable
2	1200	2.1	Instability	Instability
3	1500	1.8	Stable	Stable
4	1500	2.5	Instability	Instability
5	1800	1.5	Stable	Stable
6	1800	2.0	Instability	Instability
7	2100	1.6	Stable	Stable
8	2100	2.3	Instability	Instability
9	2400	1.7	Stable	Stable
10	2400	2.2	Instability	Instability

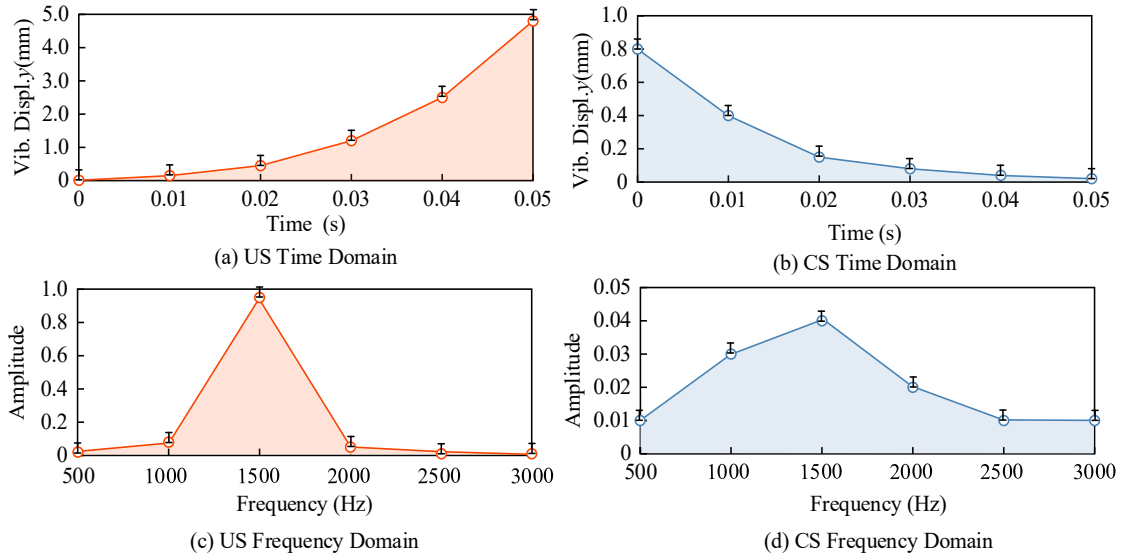
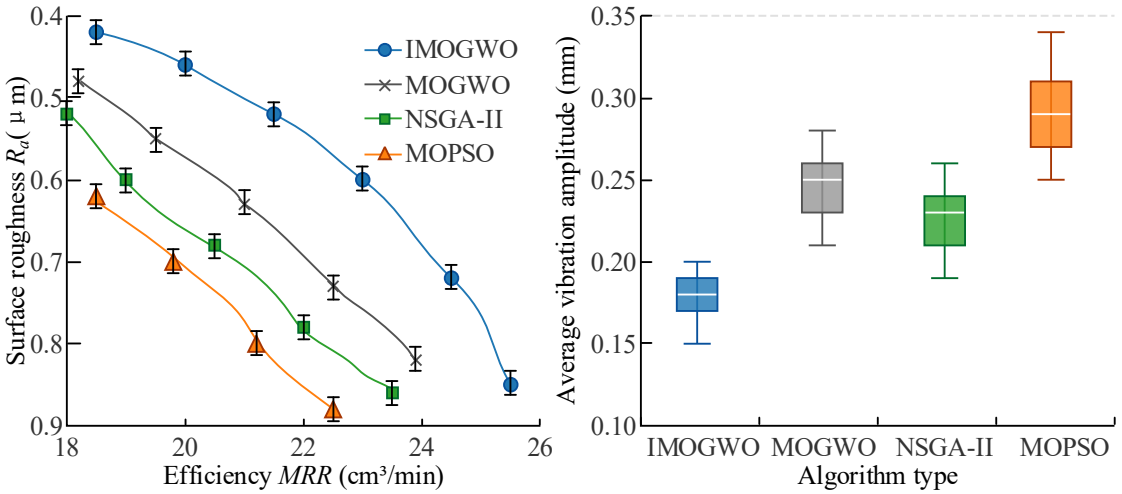


Fig. 9. Joint time-frequency domain analysis of the simulated vibration signal for a typical solution

3.3 Comprehensive Performance Evaluation of The MOGWO Algorithm in Constrained Optimization

To verify the superiority of comprehensive optimization of the IMOGWO algorithm, it was compared with MOGWO, NSGA-II, and Multi-Objective Particle Swarm Optimization (MOPSO). Figure 10 summarizes the results. From the Pareto front comparison in Figure 10(a), the IMOGWO algorithm was closest to the ideal area in the upper left corner on the efficiency-quality two-dimensional plane, and the dominant area formed was larger than the other three comparison algorithms. From the statistical comparison of vibration amplitudes in Figure 10(b), the average vibration amplitude of the solution set obtained by the IMOGWO algorithm was concentrated in the

range of 0.17-0.19mm, and its box median of 0.18mm was lower than MOGWO's 0.24mm, NSGA-II's 0.22mm and MOPSO's 0.28mm. While IMOGWO was looking for high-performance solutions, it could more effectively use stability constraints to obtain excellent parameter combinations with smaller vibrations.

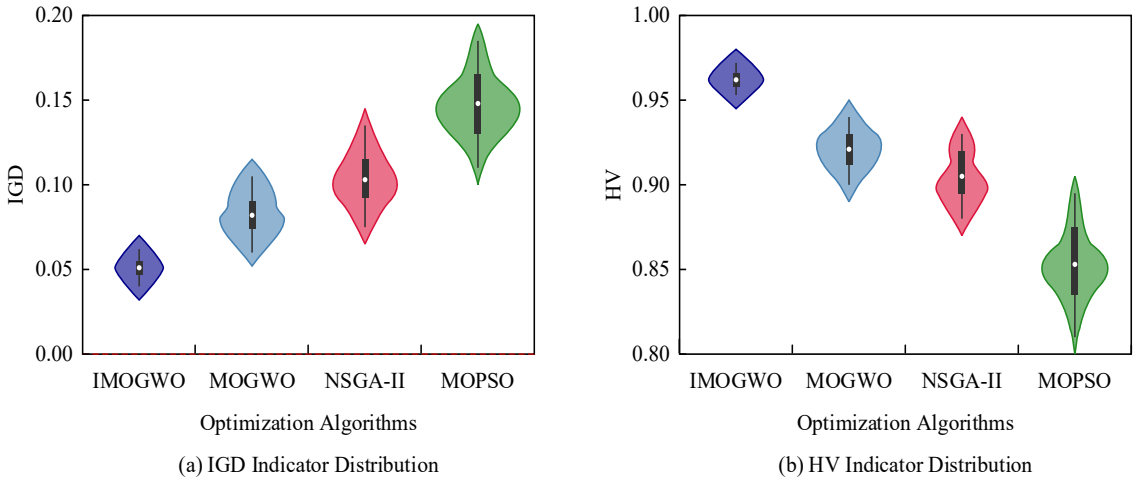


(a) Pareto front comparison in efficiency-quality dimension

(b) Vibration amplitude distribution comparison among algorithms

Fig. 10. Comparison of four algorithms on efficiency, quality, and vibration

The research continued to use Inverted Generational Distance (IGD) and Hyper-volume (HV) to compare the four algorithms. The IGD metric was used to evaluate the convergence and distribution performance of the Pareto solution set in multi-objective algorithms. There was no analytical form of the theoretical Pareto optimal frontier in this study. Therefore, the Pareto frontier was used as a reference to construct the non-dominated solution set by running all comparison algorithms multiple times and taking the union of their individual non-dominated solution sets. Firstly, the study ran IMOGWO, MOGWO, and the comparison algorithm independently 20 times each, and collected all output Pareto non dominated solutions. The study merged all solutions into one overall solution set. Then, it performed non-dominated sorting on the merged total solution set, removed dominated individuals, and used the remaining non dominated solution set as the reference Pareto front for IGD calculation. This construction method would have an impact on the computational values of IGD and was a commonly used approach in multi-objective optimization scenarios without analytical optimal solutions.



(a) IGD Indicator Distribution

(b) HV Indicator Distribution

Fig. 11. Comparison of quantitative performance metrics for the four algorithms

The HV index was used to evaluate the comprehensive performance of Pareto solution sets. Before conducting HV calculations, it was necessary to perform maximum minimum normalization on the two objective functions of material removal rate and surface roughness. Based on the process

parameters, the study searched for the boundary to determine the theoretical range of material removal rate and surface roughness. It subtracted the minimum value within the target range from the actual value of each target, and then divided by the difference between the maximum and minimum values of the target. Thus, the study mapped the values of the two targets uniformly to the range of 0 to 1. The reference point selected for HV calculation was set to (1.05, 1.05), which was outside the normalized target space. All the algorithms involved in the comparison in this study strictly adopted the maximum minimum normalization method and the same reference point (1.05, 1.05) to complete the HV calculation. The results were given in Figure 11. In Figure 11(a), after 20 independent repeated runs of the IGD index, the IGD distribution interval of the IMOGWO algorithm was 0.03-0.07, which was significantly lower than the 0.07-0.11 of MOGWO. From Figure 11(b), the HV distribution range of IMOGWO was 0.95-0.97, which was higher than that of all comparative algorithms. This showed that the IMOGWO algorithm could more comprehensively explore the safe processing space of whirl milling and provide guarantee for obtaining the best solution found under the specified parameters and computational conditions. The experimental results of algorithm ablation are shown in Table 4.

Table 4. Experimental results of algorithm ablation

unrestricted standard MOGWO	Constrained standard MOGWO	Tent chaotic mapping	Penalty function constraint	Indicator		
				IGD mean	HV mean	Average proportion of feasible solutions
×	√	√	√	0.048	0.962	97.3%
×	√	√	×	0.095	0.867	31.6%
×	√	×	√	0.074	0.913	84.5%
×	√	×	×	0.089	0.854	30.1%
√	×	×	×	0.112	0.841	27.2%

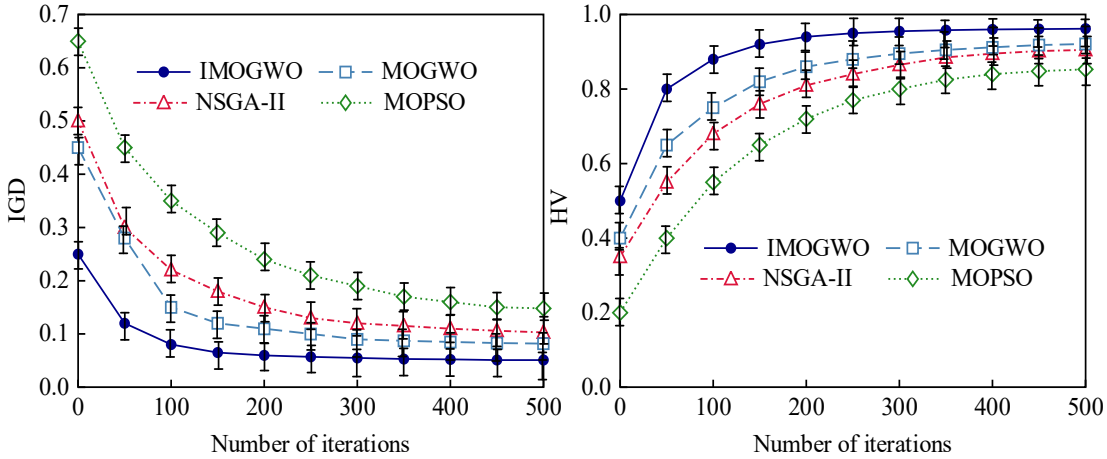
From Table 4, the fifth group was the unconstrained standard MOGWO benchmark, without introducing any improvement modules or flutter constraints. The average proportion of feasible solutions was only 27.2%, and the comprehensive optimization performance was the worst. Comparing the third and fourth groups, after introducing only penalty function constraints, the proportion of feasible solutions increased from 30.1% to 84.5%. Comparing the second and fourth groups, only using Tent chaotic mapping and disabling the penalty function resulted in limited improvement in the proportion of feasible solutions. Tent chaotic mapping only improved the initial population diversity and had little effect on constraint handling. When Tent chaotic mapping and penalty function constraints were simultaneously activated (Group 1 complete IMOGWO), the IGD mean dropped to 0.048, the HV mean reached 0.962, and the feasible solution average proportion increased to 97.3%, obtaining the most favorable overall performance. In conclusion, the performance gain of IMOGWO was the result of the combination of Tent chaotic map optimization of population initial distribution and penalty function constraint treatment of flutter boundary, not the independent contribution of a single module.

All random multi-objective algorithms in this study underwent 20 independent repeated operations to obtain the mean and standard deviation of IGD and HV. Wilcoxon rank sum test was used for statistical significance analysis, with a significance level of $p<0.05$. At the same time, the average computational cost of each algorithm in a single run was recorded. The statistical results are shown in Table 5. In Table 5, IMOGWO had the lowest IGD mean and the highest HV mean. The Wilcoxon test results showed that compared with the other three algorithms, all obtained $p<0.05$, indicating that IMOGWO demonstrated sustained performance advantages over the compared algorithms in 20 independent runs. In terms of computational overhead, the average single time consumption of IMOGWO was on the same level as the comparative algorithm, and did not bring significant computational burden.

Table 5. Comparison of statistical performance of multi objective algorithms

Algorithm	IGD (mean ± standard deviation)	HV (mean ± standard deviation)	Single average calculation time/s	Wilcoxon test (compared to IMOGWO, *p*-value)
NSGA-II	0.094±0.011	0.873±0.013	42.6	$p<0.05$
MOPSO	0.086±0.009	0.885±0.010	40.1	$p<0.05$
MOGWO	0.071±0.008	0.911±0.009	38.4	$p<0.05$
IMOGWO	0.048±0.006	0.962±0.007	41.2	/

The study ultimately compared the convergence processes of the four algorithms over 500 iterations. The population size was uniformly set at 80, with a maximum iteration of 500 generations, corresponding to an upper limit of 40000 evaluations for the total objective function. The initial population was randomly generated, and each algorithm was independently repeated 20 times. The error bars represented the fluctuations in the results of multiple runs. The evaluation frequency of the objective function was the product of the number of iterations and the population size. The results are shown in Figure 12. From Figure 12(a), the IGD value of the IMOGWO algorithm fell below 0.07 after approximately 150 iterations, outperforming the final result of the MOGWO algorithm after 500 iterations. Corresponding to only consuming 12000 objective function evaluations, the convergence quality had already exceeded the final effect after running MOGWO for 500 iterations and exhausting 40000 objective function evaluations. In Figure 12(b), the HV value of the IMOGWO algorithm rose at the fastest rate, ultimately converging to the highest level of over 0.96. Based on the two sets of convergence curves, under unified algorithm comparison conditions, IMOGWO could obtain a high-quality feasible solution set with less objective function evaluation overhead, while also considering the stability constraints of rotary milling machining, and had better optimization convergence characteristics.



(a) Convergence of IGD Indicator (b) Convergence of HV Indicator

Fig. 12. Comparison of convergence processes for the four algorithms

4. Summary

To address the dual challenges of flutter instability and low optimization efficiency in the optimization of whirl milling parameters, this study proposed an optimization scheme that integrated a physical model with an improved intelligent algorithm. The core findings derived from consistent numerical simulations were summarized as follows:

- This study established a multi-objective optimization model embedded with flutter stability hard constraints and developed the IMOGWO algorithm combining Tent chaotic mapping and an adaptive penalty mechanism for optimization solving. Constraint comparison simulations verified that the unconstrained vibration displacement diverged to nearly 5.0 mm within 0.05 s, while the CS converged rapidly below 0.1 mm within 0.03 s. The above results indicate that there is a consistent relationship between stability hard constraints and dynamic

response within the dynamic model and simulation conditions set in this paper, providing internal consistency evidence for the constructed constraint strategy (Figure 8). It should be pointed out that this result is derived from numerical simulation and cannot replace independent actual cutting experiments for physical verification of stability criteria.

- Based on 20 independent repeated runs with identical population size and total objective function evaluation budget, statistical comparison results showed that IMOGWO achieved an IGD value lower than 0.07 and an average HV value higher than 0.95. The Wilcoxon test results ($p<0.05$) indicate that IMOGWO has stable performance improvement, and under test conditions, its comprehensive optimization performance shows better optimization ability compared to MOGWO, NSGA-II, and MOPSO (Table 5).
- Convergence analysis indicated that IMOGWO obtained higher-quality Pareto solutions at approximately 150 iterations, corresponding to only 12,000 objective-function evaluations, which outperformed the final optimized results of MOGWO after 500 iterations (40,000 objective-function evaluations). This reflected favorable computational performance of IMOGWO under unified function-evaluation criteria (Figure 12).
- Ablation experiments further verified the internal improvement mechanism of the proposed algorithm. The excellent performance of IMOGWO originated from the synergistic optimization effect of Tent chaotic mapping for improving initial population diversity and the adaptive penalty mechanism for handling nonlinear stability constraints, rather than the contribution of a single module (Table 4).

In summary, the proposed optimization scheme alleviated the conflicting relationship between machining performance and chatter stability within the given simulation parameter range, offering a feasible alternative for whirl-milling parameter optimization. All conclusions in this study were strictly limited to numerical simulation results. This work did not consider practical uncertain factors including tool wear and thermal deformation in actual cutting processes. Thus, the findings could not be directly applied to general engineering scenarios. Future work will conduct physical cutting experiments to further improve the practical robustness of the proposed optimization framework.

Fundings

The research is supported by Shandong Huayu University of Technology CNC tool manufacturing process research and development center (PT2025KJX001).

References

[1] Jiang X, Wei Y, Zhou J, Zhan K, Ding Z, Liang SY. Residual stress generation and evaluation in milling: a review. The International Journal of Advanced Manufacturing Technology. 2023;126(9):3783-3812. https://doi.org/10.1007/s00170-023-11394-1

[2] Guo Q, Wang W, Jiang Y, Sun Y, Yang Z, Luo C, Chen M. A high-efficient numerical control (NC) turning method for double-enveloping worms using spindle forward-and reverse-rotating strategy. Proceedings of the Institution of Mechanical Engineers, Part C: Journal of Mechanical Engineering Science. 2026;240(3):743-764. https://doi.org/10.1177/09544062251383774

[3] Feng C, Qin E, Li W, Li M, Su J, Xu X. Energy consumption and surface roughness modelling for multi-objective optimisation of machining processes. The International Journal of Advanced Manufacturing Technology. 2024;133(9):5065-5087. https://doi.org/10.1007/s00170-024-14043-3

[4] Zhang Z, Yang Y, Li G, Qi Y, Yue C, Hu Y, Li Y. Machining accuracy reliability evaluation of CNC machine tools based on the milling stability optimization. The International Journal of Advanced Manufacturing Technology. 2023;124(11):4057-4074. https://doi.org/10.1007/s00170-022-08832-x

[5] Hassien ASA, Abosetah NSA. Smart Algorithm Applications in Mechanical Engineering and Physical Sciences for Optimizing Systems and Materials. PERFECT: Journal of Smart Algorithms. 2025;2(1):7-15. https://doi.org/10.62671/perfect.v2i1.50

[6] Waqas M, Naseem A. Artificial intelligence in sustainable industrial transformation: A comparative study of industry 4.0 and industry 5.0. FinTech and Sustainable Innovation. 2025;1:A2-A2. https://doi.org/10.47852/bonviewFSI52025321

[7] Guo Q, Wang M, Xie J, Wang Y. The comprehensive improvement of surface integrity in whirlwind milling a large screw. Proceedings of the Institution of Mechanical Engineers, Part B: Journal of Engineering Manufacture. 2023;237(4):532-541. https://doi.org/10.1177/09544054221102206

[8] Chen X, Shen D, Ou C, Ma J, Lu J, Liao X. Optimization of machining efficiency and side quality in irregular sheet metal parts milling based on improved multi-objective seagull optimization algorithm. The International Journal of Advanced Manufacturing Technology. 2024;135(5):2755-2776. https://doi.org/10.1007/s00170-024-14540-5
[9] Yu Y, Ji X, Dai S, Zuo D, Song S. Profile design and simulation verification of hard whirling tool for ZC1 worm machining. Proceedings of the Institution of Mechanical Engineers, Part B: Journal of Engineering Manufacture. 2023;237(8):1220-1229. https://doi.org/10.1177/09544054221123475
[10] Kumar G, Goyal KK, Batra NK, Mehdi H. Optimizing reconfigurable manufacturing system configuration selection with multi-objective grey wolf optimization. International Journal on Interactive Design and Manufacturing (IJIDeM). 2025;19(8):5567-5582. https://doi.org/10.1007/s12008-024-02150-0
[11] Ekanem I, Ikpe A, Ite O. Adoption of Multi-Objective Grey Wolf Optimization (MOGWO) for Effective Analysis and Classification of Crystal Structures in Materials Science. Metaheuristic Algorithms with Applications. 2025;2(1):1-35.
[12] Gopi T, Goud PS, Abhishek K, Sateesh N. A hybrid multi-optimization of cutting rate and surface roughness using PCA-based improved-GWO in precise CNC turning of AA2014. International Journal on Interactive Design and Manufacturing (IJIDeM). 2025;19(6):4113-4121. https://doi.org/10.1007/s12008-024-02031-6
[13] Ahmed KS, Sendur GK, Bediz B. Integrated design optimization of a motorized active magnetic bearing spindle for micro-milling applications. Journal of Mechanical Science and Technology. 2025;39(4):2015-2027. https://doi.org/10.1007/s12206-025-0327-x
[14] Boddu JR, Kotaiah KR, Chalapathi PV, Shaik JH. Optimization of design for the high precision end mill spindles to improve stability of effective cutting process. International Journal on Interactive Design and Manufacturing (IJIDeM). 2025;19(1):165-173. https://doi.org/10.1007/s12008-023-01526-y
[15] Wei J, Zheng Q, Yan W, Li H, Chi Z, Jiang B. Probabilistic analysis of blade flutter based on particle swarm optimization-deep extremum neural network. International Journal of Turbo & Jet-Engines. 2025;42(1):99-114. https://doi.org/10.1515/tjj-2024-0041
[16] Hirano K, Sato T, Suzuki N. Real-time prediction of material removal rate for advanced process control of chemical mechanical polishing. CIRP Annals. 2024;73(1):269-272. https://doi.org/10.1016/j.cirp.2024.04.028
[17] Devlukia S, Hammond L, Malik K. Is surface roughness of direct resin composite restorations material and polisher-dependent? A systematic review. Journal of Esthetic and Restorative Dentistry. 2023;35(6):947-967. https://doi.org/10.1111/jerd.13102
[18] Heidari A, Imani DM, Khalilzadeh M, Sarbazvatan M. Green two-echelon closed and open location-routing problem: application of NSGA-II and MOGWO metaheuristic approaches. Environment, Development and Sustainability. 2023;25(9):9163-9199. https://doi.org/10.1007/s10668-022-02429-w
[19] Torabi A, Yosefvand F, Shabanlou S, Rajabi A, Yaghoubi B. Optimization of integrated operation of surface and groundwater resources using multi-objective grey wolf optimizer (MOGWO) algorithm. Water resources management. 2024;38(6):2079-2099. https://doi.org/10.1007/s11269-024-03744-9
[20] Asigri P, Anto EK, Kwegyir D, Effah FB. ENHANCED MULTI-OBJECTIVE GREY WOLF OPTIMIZATION USING ADAPTIVE DIVERSITY TUNING AND LEVY FLIGHTS. Carpathian Journal of Electrical Engineering. 2024;18(1):7-35. https://doi.org/10.34302/CJEE/TKYD3692